

Fulde-Ferrell-Larkin-Ovchinnikov States in Two-Band Superconductors

Takeshi Mizushima^{1,2*}, Masahiro Takahashi³, and Kazushige Machida¹

¹*Department of Physics, Okayama University, Okayama 700-8530, Japan*

²*Department of Physics and Astronomy, Northwestern University, Evanston, Illinois 60208, USA*

³*Department of Physics, Gakushuin University, Tokyo 171-8588, Japan*

We examine the possible phase diagram in an H - T plane for Fulde-Ferrell-Larkin-Ovchinnikov (FFLO) states in a two-band Pauli-limiting superconductor. We here demonstrate that, as a result of the competition of two different modulation length scales, the FFLO phase is divided into two phases by the first-order transition: the Q_1 - and Q_2 -FFLO phases at the higher and lower fields. The Q_2 -FFLO phase is further divided by successive first order transitions into an infinite family of FFLO subphases with rational modulation vectors, forming a *devil's staircase structure* for the field dependences of the modulation vector and paramagnetic moment. The critical magnetic field above which the FFLO is stabilized is lower than that in a single-band superconductor. However, the tricritical Lifshitz point L at T_L is invariant under two-band parameter changes.

Introduction.— Owing to the fundamental significance of the coexistence of superconductivity and magnetism, Fulde-Ferrell-Larkin-Ovchinnikov (FFLO) states^{1,2} have attracted much attention in the fields of condensed matter,³ cold atoms,^{4–8} and neutron stars.⁹ Still FFLO remains elusive in spite of extensive experimental and theoretical investigations in a wide range of fields. The emergence of the FFLO state via the second-order transition is accompanied by the Jackiw-Rebbi soliton¹⁰ by which the Pauli paramagnetic moment is neatly accommodated.¹¹ The soliton provides a generic key concept for the common understanding of the essential physics of the FFLO phase in a single-band superconductor, incommensurate structures,^{12,13} and fermionic excitations bound at topological defects of a superconductor.¹⁴

Multiband effects with multiple sheets of Fermi surfaces are observed in a variety of superconductors, such as MgB₂, iron-based superconductors, and Sr₂RuO₄ to mention a few.^{15,16} It has been proposed that multi-band effects are accompanied by exotic superconductivity.^{17–20} It is now recognized that the multiband superconductor is the rule rather than the exception. Nevertheless, in contrast to those in a single-band superconductor,³ the FFLO phases in multiband systems have not been clarified so far, except in few studies.^{21–23}

Results of several recent experiments have collectively urged us to investigate the FFLO phases in multibands: The observations of strong Pauli effects in iron pnictides^{24–28} and of a strange phase boundary line, $\frac{dT_{LO}}{dH} > 0$ (T_{LO} is the BCS-FFLO transition line), in another multiband heavy-fermion superconductor, CeCoIn₅, for $H \parallel ab$,²⁹ which is in contrast with a conventional phase diagram with $\frac{dT_{LO}}{dH} < 0$ (see the inset of Fig. 1 and Refs.³ and³⁰).

In a single-band superconductor, the self-organized periodic structure of the FFLO state is a direct consequence of

the synergistic effect between spin paramagnetism and superconductivity with the spontaneous breaking of the translational symmetry. The spatial modulation is characterized by the single length scale Q^{-1} , proportional to the Fermi velocity $Q^{-1} \propto v_F$.¹¹ Multiband superconductivity is characterized by multicomponent pair potentials. In the absence of interband coupling, the γ band ($\gamma = 1, 2$) independently has its own favored FFLO modulation Q_γ^{-1} . When the interband coupling becomes finite, however, two pair potentials are no longer independent and the coupling gives rise to the competition of multiple length scales self-consistently determined, Q_γ^{-1} .

In this Letter, we try to establish the essential features of FFLO characteristic of multiband superconductors, which are

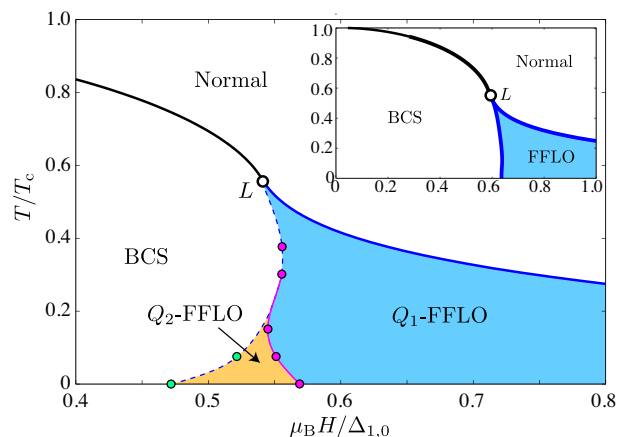


Fig. 1. (color online) Phase diagram in an H - T plane. The thick (thin) lines indicate the second (first) -order transition lines. The Q_2 -FFLO phase is subdivided into a family of FFLO subphases. The open circle is the Lifshitz point L at (T_L, H_L) . The order of the dashed line is undetermined. The inset describes the phase diagram in a single-band system.¹¹

*E-mail: mizushima@mp.okayama-u.ac.jp

absent in a single-band case,¹¹ and examine the possible phase diagram for FFLO phases. The resulting phase diagram is summarized in Fig. 1, where our main outcome is threefold: (i) The FFLO phase is divided into two main phases by the first-order transition, each having a different modulation periodicity. The Q_1 -FFLO phase stabilized in the higher field is understandable with the single modulation vector Q_1 of the major band ($\gamma = 1$). The Q_2 -FFLO phase in Fig. 1 is a result of the competing effect of two different length scales $Q_1^{-1} \neq Q_2^{-1}$ and is unique to two-band superconductors. (ii) The Q_2 -FFLO phase is further subdivided by first-order transitions into a family of FFLO subphases with the sequence of rational modulation vectors $Q_2/(2n+1)$ ($n \in \mathbb{Z}$). This successive first-order phase transition exhibits a *devil's staircase structure* for the modulation period and magnetization. (iii) The onset field of the FFLO phase is lower than the Lifshitz point H_L owing to the interband effect and the phase boundary indicates a positive slope $\frac{dT_{10}}{dH} > 0$.

Formulation.— We consider spin- $\frac{1}{2}$ fermions ($\sigma = \uparrow, \downarrow$) in two bands $\gamma = 1, 2$ under a magnetic field H , interacting through an attractive s -wave interaction $g_{\gamma\gamma'} = g_{\gamma'\gamma} < 0$. We deal with a quasi-one-dimensional (Q1D) system along the FFLO modulation vector (\hat{z} -axis). This is a minimal extension of a single-band theory.^{11,31} The quasiparticles with the wave function $\varphi_{v,\gamma} = [u_{v,\gamma}, v_{v,\gamma}]^T$ and energy E_γ in the γ -band are obtained by solving the Bogoliubov-de Gennes (BdG) equation³²

$$\begin{bmatrix} \xi_\gamma(z) & \Delta_\gamma(z) \\ \Delta_\gamma^*(z) & -\xi_\gamma^*(z) \end{bmatrix} \varphi_{v,\gamma}(z) = E_{v,\gamma} \varphi_{v,\gamma}(z), \quad (1)$$

where $\varphi_{v,\gamma}$ must fulfill $\int dz \varphi_{v,\gamma}^\dagger \varphi_{v,\gamma} = 1$. In this paper, we set $\hbar = k_B = 1$. The single-particle Hamiltonian density is $\xi_\gamma(z) = \frac{1}{2M_\gamma} (-i\frac{d}{dz} + A)^2 - \mu_\gamma - \mu_B H$ with the mass M_γ . The chemical potentials μ_γ are parameterized as $\mu_1 = E_F + \mu_{12}/2$ and $\mu_2 = E_F - \mu_{12}/2$. Since we are interested in the strong Pauli limit, the vector potential A is supposed to be spatially uniform, neglecting the orbital effect.³⁰ Note that the orbital effect can be suppressed in low-dimensional superconductors.^{33,34}

The BdG equation Eq. (1) is self-consistently coupled with the gap equation in the γ -band given by

$$\Delta_\gamma(z) = \sum_{\gamma'} g_{\gamma\gamma'} \Phi_{\gamma'}(z), \quad (2)$$

where $\Phi_\gamma(z) = \sum_v u_{v,\gamma}(z) v_{v,\gamma}^*(z) f(E_{v,\gamma})$ describes the Cooper pair amplitude in the γ -band with the distribution function at the temperature T , $f(E) = 1/(e^{E/T} + 1)$.

In Eq. (2), $g_{12} = g_{21}$ denotes the amplitude of the interband pair tunneling. Although we examined several sets of parameters ($g_{12}/g_{11}, g_{22}/g_{11}, \mu_2/\mu_1$),³⁵ we here concentrate on the set (0.1, 0.6, 0.5), where the density of states (DOS) at the Fermi surface of normal electrons, \mathcal{N}_γ , is dominated by the minor band $\mathcal{N}_2/\mathcal{N}_1 = 2$. Thus, the Fermi velocity ratio is $v_{F,2}/v_{F,1} = 1/\sqrt{2}$ in our 1D parabolic dispersion. We here

assume $M_1 = M_2$ because the deviation merely alters the ratios of $v_{F,2}/v_{F,1}$ and $\mathcal{N}_2/\mathcal{N}_1$. This results in $\Delta_{2,0}/\Delta_{1,0} \approx 0.5$ at $T = H = 0$, where $\Delta_{\gamma,0} \equiv \Delta_\gamma(T = 0)$. Namely, the band $\gamma = 1$ ($= 2$) is major (minor) in its gap.

We here consider a 1D modulation with the period L ,

$$\Delta_\gamma(z + L/2) = e^{i\chi} \Delta_\gamma(z), \quad (3)$$

where $\chi = \pi(2\pi)$ corresponds to FFLO (BCS) states. This imposes the periodic boundary condition on quasiparticle wave functions, $\varphi_{v,\gamma}(z + pL/2) = e^{ikR} e^{i\chi\sigma z/2} \varphi_{v,\gamma}(z)$, where $k = \frac{2\pi q}{LN_L}$ is the Bloch vector and R denotes the Bravais lattice vector that satisfies $kR = \pi pq/N_L$ with $p, q \in \mathbb{Z}$. Hence, we self-consistently solve Eq. (1) coupled with the gap equation (2) in the interval $z \in [0, L/2]$. The BdG equation Eq. (1) is numerically diagonalized with the finite element method implemented with the discrete variable representation.³⁵ In this work, we deal with $L/\xi < 40$, where $\xi = v_{F,1}/\Delta_{1,0}$ is the coherence length.

Sequence of FFLO states.— Within the condition in Eq. (3), there exists a family of FFLO states as a consequence of the interplay between two bands. To clarify this, we start with the Fourier expansion in FFLO states, $\Delta_\gamma(z) = \sum_{m_\gamma \in \mathbb{Z}} e^{iq_\gamma(2m_\gamma+1)z} \Delta_\gamma^{(m_\gamma)}$. Note that the symmetry requires $Q(2m-1) \equiv q_1(2m_1-1) = q_2(2m_2-1)$. Then, $\Delta_{1,2}(z)$ is expanded with $Q = \frac{2\pi}{L}$ as

$$\Delta_\gamma(z) = \sum_{m \in \mathbb{Z}} e^{iQ(2m-1)z} \Delta_\gamma^{(m)}. \quad (4)$$

In a single-band superconductor with $\Delta_2 = 0$, an isolated kink state characterized by $\Delta_1^{(m)} = \frac{\Delta_{1,0}}{2|m-1|}$ is stabilized at the critical field $\mu_B H = \frac{2}{\pi} \Delta_{1,0}$.¹¹ The higher Fourier components with $|m| \geq 2$ disappear as H increases and the spatial modulation results in the sinusoidal form $\Delta_1(z) \propto \sin(Qz)$. The field dependence of Q follows the relation $Q \sim 2\mu_B H/v_F$ in the high-field limit.¹¹ In the case of two-band superconductors, the modulation vector Q_γ of $\Delta_\gamma(z)$ is determined as a result of the competition between two bands, where the $\gamma = 1$ ($\gamma = 2$) band favors the modulation vector $Q_1 \propto v_{F,1}^{-1} \propto \mu_1^{-1}$ ($Q_2 \propto v_{F,2}^{-1} \propto \mu_2^{-1}$) and $Q_1 < Q_2$ in our system.

Figure 2 shows the thermodynamic potential $\Omega = -\sum_{\gamma,\gamma'} g_{\gamma\gamma'} \langle \Phi_\gamma^*(z) \Phi_{\gamma'}(z) \rangle + \sum_{v,\gamma} \{ E_{v,\gamma} \langle |u_{v,\gamma}|^2 \rangle - T \ln(1 + e^{-E_{v,\gamma}/T}) \}$ for a fixed FFLO period $Q^{-1} \equiv L/2\pi$, where $\langle \dots \rangle$ denotes the spatial average over the system. We evaluate $\Omega(Q)$ with self-consistent solutions of Eqs. (1) and (2). It is seen from Fig. 2(a) that $\Omega(Q)$ has several local minima, $\frac{\partial \Omega}{\partial Q} = 0$ and $\frac{\partial^2 \Omega}{\partial Q^2} \geq 0$, in the lower-temperature regime. The local minimum with the largest Q ($\xi Q \sim 0.8$) corresponds to $Q_1 \xi$, which is favored by the major band, and the other minima with small Q 's follow $Q_2/(2n+1)$ with $n \geq 1$. This is in contrast to the higher-temperature regime shown in Fig. 2(b), where only a single minimum exists, which monotonically shifts towards the shorter L as H increases. The FFLO period Q tends to $Q_1 \sim \mu_B H/v_{F,1}$ at high fields, which is understandable from the single-band picture.

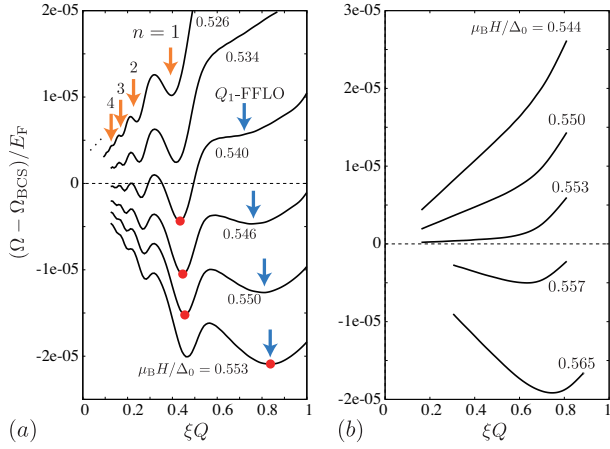


Fig. 2. (color online) Thermodynamic potential Ω with respect to the FFLO period $Q \equiv 2\pi/L$ at $T/T_c = 0.075$ (a) and 0.30 (b) for various magnetic fields H .

To clarify the distinction between the Q_1 - and Q_2 -FFLO states, we show $\Delta_\gamma(z)$ at $\mu_B H/\Delta_{1,0} = 0.546$ and $T = 0.075T_c$ in Figs. 3(a) and 3(b), which correspond to the local minima with the largest and second largest Q values, respectively. Figures 3(e)-3(g) show the Fourier components $\Delta_2^{(m)}$ in Eq. (4). It is seen from Figs. 3(a) and 3(e) that the local minimum state with $Q\xi = 0.76$ is characterized by a single peak at $m = 1$, corresponding to $Q \equiv \frac{2\pi}{L} \sim Q_1$. In this sense, we refer to this phase as the Q_1 -FFLO phase. In the Q_1 -FFLO phase, the Pauli paramagnetic moment $\mathcal{M}_\gamma = \langle m_\gamma \rangle = \sum_\nu [\langle |u_{\nu,\gamma}|^2 \rangle f(E_{\nu,\gamma}) - \langle |v_{\nu,\gamma}|^2 \rangle f(-E_{\nu,\gamma})]$ in the γ -band accumulates in the FFLO node at which the midgap bound states with spin \uparrow (\downarrow) are formed inside (outside) of the Fermi surface as the Jackiw-Rebbi soliton. Hence, the spatial modulation of $\mathcal{M}_{\gamma=2}$ is characterized by a single $2Q$, as shown in Figs. 3(c) and 3(h), where the spatial uniform contribution of \mathcal{M}_γ with $n = 0$ is omitted. Here, $\mathcal{M}_\gamma(z)$ is expanded with $Q = \frac{2\pi}{L}$ as $\mathcal{M}_\gamma(z) = \sum_{m \in \mathbb{Z}} e^{i2mQz} \mathcal{M}_\gamma^{(m)}$.

In the low- T regime, the contributions of the minor band become competitive, giving rise to the appearance of several local minima in addition to the Q_1 -FFLO state, as shown in Fig. 2(a). This competing effect is also reflected in the phase diagram shown in Fig. 1, where the critical field above which the Q_2 -FFLO phase appears is much lower than $h_{\text{crit}} = \frac{2}{\pi}\Delta$ in a single-band system.¹¹ To understand the structure of the Q_2 -FFLO phase, in Figs. 3(b) and 3(g), we display the spatial profile of $\Delta_{1,2}(z)$ with $Q\xi = 0.27$ at $\mu_B H/\Delta_0 = 0.546$, corresponding to the local minimum labeled as $n = 2$ in Fig. 2(a). In the regime around the critical field in two-band systems, Q_2^{-1} is comparable to the coherence length $Q_2^{-1} \sim \xi$, whereas $Q_1^{-1} \gg \xi$, since $v_{F,1} > v_{F,2}$. The FFLO phase with the single modulation vector Q_2 is not favorable because of the loss of condensation energy, and the stability of the Q_1 -FFLO phase requires a higher magnetic field. As shown in Eq. (4), however, it is possible to realize a family of Q_2 's, such as $Q_2/3, Q_2/5, \dots$ in

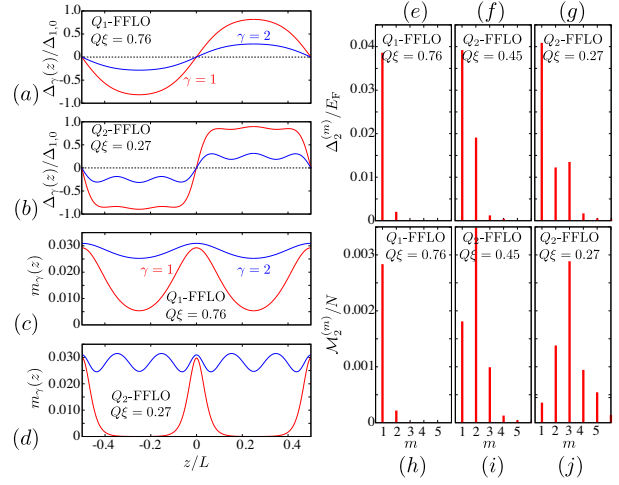


Fig. 3. (color online) Spatial profiles of $\Delta_\gamma(z)$ and $m_\gamma(z)$ in Q_1 - and Q_2 -FFLO states at $T/T_{c0} = 0.075$ and $\mu_B H/\Delta_{1,0} = 0.546$: $Q\xi = 0.76$ (a, c) and 0.27 (b, d). Histogram of corresponding Fourier components $\Delta_2^{(m)}$ (e-g) and $\mathcal{M}_2^{(m)}$ (h-j) in the $\gamma=2$ band.

two-band systems. It is clearly seen from Figs. 3(b) and 3(g) that $\Delta_{1,2}(z)$ with $Q\xi = 0.27$ is composed of multiple modulation vectors, $3Q \sim 0.91\xi^{-1}$ ($m = 2$) and $5Q \sim 1.4\xi^{-1}$ ($m = 3$) in addition to $Q \sim 0.27\xi^{-1}$ ($m = 1$). Although the modulation vector favored in the minor band is estimated as $Q_2 \approx 1.4\xi^{-1}$, the optimal wave number $Q\xi = 0.27$ that determines the overall FFLO period corresponds to $Q \sim Q_2/5$, and the induced components $3Q$ and $5Q$ are found to be $3Q_2/5$ and Q_2 , respectively.

In the series of local minima labeled as $n = 1, 2, \dots$ in Fig. 2(a), $\Delta_\gamma(z)$ are composed of the overall modulation vector $Q \approx Q_2/(2n+1)$ and the induced components $(2m-1)Q_2/(2n+1)$ with $m = 1, 2, \dots$. This family of $Q \approx Q_2/(2n+1)$ is referred to as the Q_2 -FFLO phase, which can be stabilized in the lower- H and lower- T regimes in Fig. 1. The multiple- Q modulated structure in the Q_2 -FFLO phase is clearly reflected in the spatial profile of the Pauli paramagnetic moment displayed in Fig. 3(d), and the Fourier components in Figs. 3(i) and 3(j) have sharp peaks at $2Q_2$. It is also seen from Fig. 2(a) that the family of the Q_2 -FFLO phase undergoes the first-order transition to the Q_1 -FFLO phase as H increases.

Devil's staircase structure.— The appearance of the Q_2 -FFLO phase is a consequence of the competition of the two length scales Q_1^{-1} and Q_2^{-1} , which is unique to multiband superconductors. We here discuss the thermodynamic stability of the Q_1 and Q_2 phases with respect to H . Figure 4(a) shows the quasiparticle dispersion in the minor band ($\gamma = 2$) of the Q_1 -FFLO state with $Q\xi = 0.76$ and the $n = 1$ Q_2 -FFLO state with $Q\xi = 0.45$ at $T = 0.075T_c$ and $\mu_B H = 0.546\Delta_{1,0}$. The band structure at approximately $E_{k,\gamma} = -\mu_B H$ is interpreted as the lattice of the Jackiw-Rebbi solitons bound at the FFLO nodes, responsible for the paramagnetic moment.

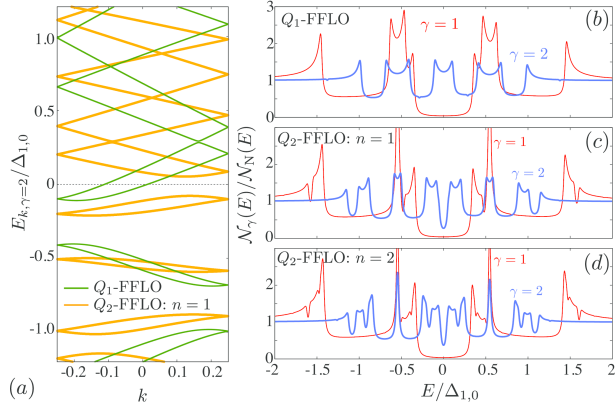


Fig. 4. (color online) (a) Dispersion in the reduced zone for the $\gamma=2$ band of the Q_1 -FFLO state with $Q\xi=0.76$ and $n=1$ Q_2 -FFLO state with $Q\xi=0.45$. DOS of Q_1 -FFLO state with $Q\xi=0.76$ (b) and Q_2 -FFLO state with $Q\xi=0.45$ (c) and $Q\xi=0.27$ (d). The other parameters are the same as those in Fig. 3

The most distinct structure between the Q_1 - and Q_2 -FFLO phases is seen around $E_{k,\gamma} = 0$. In the Q_1 -FFLO phase, the dispersion crosses $E_{k,\gamma} = 0$, giving rise to a large amount of the zero-energy DOS and paramagnetic moment as shown in Figs. 3(b) and 4(b). The DOS is defined as $N_\gamma(E) = \sum_\nu [|\mu_{\nu,\gamma}|^2 \delta(E - E_{\nu,\gamma}) + |v_{\nu,\gamma}|^2 \delta(E + E_{\nu,\gamma})]$. In the case of the Q_2 -FFLO phase with $n=1$, $\Delta_2(z)$ is mostly composed of two different Fourier components, $Q_2/3$ and Q_2 , as shown in Fig. 3(f), while $\Delta_2(z)$ in the Q_1 -FFLO phase is described by a single Q . Hence, the original band in the Q_2 -FFLO state with $Q = Q_2/3$ is folded back into a small reduced Brillouin zone, reflecting the mixed component with the larger modulation vector $3Q = Q_2$. Then, the band gap opens at approximately zero energy, which reduces $N_2(E = 0)$ but gains condensation energy. Hence, the energetics of the FFLO phases is simply understandable as the competition between the Q_1 -FFLO phase with zero-energy DOS and the Q_2 -FFLO phase with condensation energy.

Figure 5(a) shows a summary of the field dependence of the modulation vector $Q \equiv 2\pi/L$ at $T = 0$, where the symbols “ \times ” and “+” denote the metastable solutions. The ground state denoted by filled circles is determined by minimizing $\Omega(L)$. The field dependence of $Q_{1,2}$ in a single-band superconductor is plotted as a reference, where Q_1 and Q_2 are estimated using $(v_{F,1}, \Delta_{1,0})$ and $(v_{F,2}, \Delta_{2,0})$, respectively.¹¹ It is shown in Fig. 5(a) that the $Q(H)$ curve is understandable with two competing modulation vectors, Q_1 and Q_2 . The branch with the largest Q , called the Q_1 -FFLO phase, follows $Q_1(H)$, which is dominated by the $\gamma = 1$ band with $v_{F,1}$ and $\Delta_{1,0}$, whereas the branches with the smaller Q 's are categorized into the family of the Q_2 -FFLO phases with an infinite rational vector $Q_2/(2n + 1)$ ($n = 1, 2, \dots, \infty$). Thus, Q and M in the ground state have a step structure, called the *devil's staircase* structure.^{36,37} At $\mu_B H = 0.552\Delta_{1,0}$, the Q_2 -FFLO phase undergoes the first-order transition to the Q_1 -FFLO phase with the

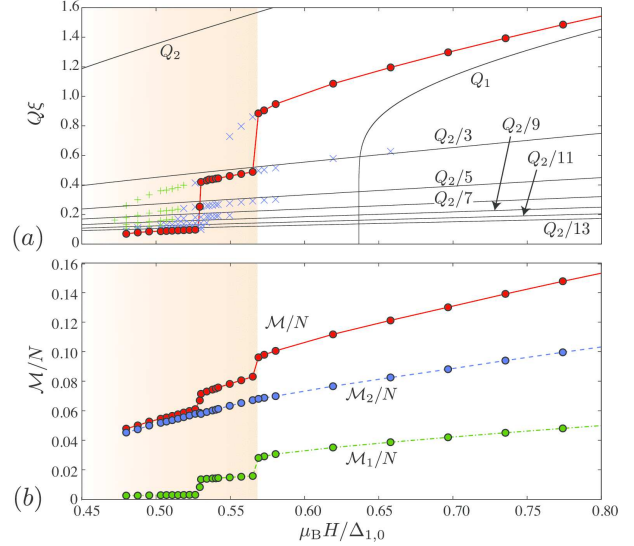


Fig. 5. (color online) Field dependence of the FFLO modulation Q (a) and the magnetization M/N (b) at $T = 0$. The symbols \times and $+$ indicate the metastable states in $\Omega(Q)$, where $\Omega(+)$ is higher than that in the BCS phase. The shaded area denotes the Q_2 -FFLO phase, where the transition between BCS and Q_2 -FFLO phases takes place at approximately $\mu_B H/\Delta_0 \approx 0.45$.

shorter FFLO period.

KFe₂As₂ is a strongly Pauli-limited superconductor with α -, β -, ζ - and ϵ -bands.^{26,27} A minor (major) gap forms on the α -, β -, and ζ - (ϵ) bands with a relatively larger (smaller) Fermi velocity, which leads to $Q_{\alpha\beta\zeta} < Q_\epsilon$ or $Q_2 < Q_1$ in the present context. Note that the $Q_2 < Q_1$ case inevitably has a critical field at which the $Q_2(H)$ curve crosses $Q_1(H)$. The lower-field regime with $Q_2 \neq 0$ and $Q_1 = 0$ is dominated by the minor band, in which the Q_2 -FFLO phase is stabilized. The higher-field regime with $Q_2 < Q_1$ turns to the Q_1 -FFLO phase via the first order transition.³⁵ Hence, the emergence of the Q_2 -FFLO phase is a generic feature in two-band Pauli-limiting superconductors, but the Q_2 -FFLO phase is not divided into sub-phases and the devil's staircase is absent, when $Q_2/Q_1 \lesssim 1$. To fully understand KFe₂As₂, however, we have to take account of the orbital effect. The interplay between vortices and FFLO states in multiband systems remains as a future problem. Note that the generalized WHH approach has recently made the Pauli-limit effect of KFe₂As₂ questionable.³⁸

Conclusions.— We have examined the multiband effects on FFLO phases and revealed that generic and nontrivial features are absent in a single-band case. Our calculation is based on a minimal model extended from a canonical 1D FFLO Hamiltonian.¹¹ We have demonstrated that the FFLO phase diagram in the H vs T plane is divided into two main subphases by the first order transition, where the Q_2 -FFLO phase in the lower- H regime is further subdivided, giving rise to a devil's staircase in physical quantities. Yet, remarkably, the tricritical Lifshitz point L at $T_L/T_c = 0.561\dots$, where the normal, FFLO, and uniform BCS phases meet,^{37,39} is invariant even in the

multiband case, as shown in Fig. 1, independent of any of the parameters g_{12}/g_{11} , g_{22}/g_{11} , and μ_1/μ_2 .³⁵ This is a generic feature observed in various systems.^{40–44} The present findings on the FFLO state are also applicable to imbalanced superfluids with two chains^{45,46} in ultracold atoms.

Acknowledgments This work was supported by JSPS (Grant Nos. 21340103, 23840034, and 25800199) and “Topological Quantum Phenomena” (No. 22103005) KAKENHI on innovation areas from MEXT.

- 1) P. Fulde and R. A. Ferrell, Phys. Rev. **135**, A550 (1964).
- 2) A. I. Larkin and Y. N. Ovchinnikov, Sov. Phys. JETP **20**, 762 (1965).
- 3) Y. Matsuda and H. Shimahara, J. Phys. Soc. Jpn. **76**, 051005 (2007).
- 4) M. W. Zwierlein, A. Schirotzek, C. H. Schunck, and W. Ketterle, Science **311**, 492 (2006).
- 5) Y. Liao, A. S. C. Rittner, T. Paprotta, W. Li, G. B. Partridge, R. G. Hulet, S. K. Baur, and E. J. Mueller, Nature **467**, 567 (2010).
- 6) T. Mizushima, K. Machida, and M. Ichioka, Phys. Rev. Lett. **94**, 060404 (2005).
- 7) D. E. Sheehy and L. Radzihovsky, Ann. Phys. (N.Y.) **322**, 1790 (2007).
- 8) Z. Cai, Y. Wang, and C. Wu, Phys. Rev. A **83**, 063621 (2011).
- 9) R. Casalbuoni and G. Nardulli, Rev. Mod. Phys. **76**, 263 (2004).
- 10) R. Jackiw and C. Rebbi, Phys. Rev. D **13**, 3398 (1976).
- 11) K. Machida and H. Nakanishi, Phys. Rev. B **30**, 122 (1984).
- 12) W. P. Su, J. R. Schrieffer, and A. J. Heeger, Phys. Rev. Lett. **42**, 1698 (1979).
- 13) H. Takayama, Y. R. Lin-Liu, and K. Maki, Phys. Rev. B **21**, 2388 (1980).
- 14) T. Mizushima, K. Machida, and M. Ichioka, Phys. Rev. Lett. **95**, 117003 (2005) and references therein.
- 15) L. Komendová, Y. Chen, A. A. Shandenko, M. V. Milošević, and F. M. Peeters, Phys. Rev. Lett. **108**, 207002 (2012).
- 16) Y. Maeno, S. Kittaka, T. Nomura, S. Yonezawa, and K. Ishida, J. Phys. Soc. Jpn. **81**, 011009 (2012).
- 17) E. Babaev and M. Speight, Phys. Rev. B **72**, 180502(R) (2005).
- 18) J. Carlström, E. Babaev, and M. Speight, Phys. Rev. B **83**, 174509 (2011).
- 19) T. Hirano, K. Takamori, M. Ichioka, and K. Machida, J. Phys. Soc. Jpn. **82**, 063708 (2013).
- 20) V. G. Kogan and J. Schmalian, Phys. Rev. B **83**, 054515 (2011).
- 21) A. Gurevich, Phys. Rev. B **82**, 184504 (2010).
- 22) A. Ptok and D. Crivelli, J. Low Temp. Phys. **172**, 226 (2013).
- 23) A. Ptok, Eur. Phys. J. B **87**, 2 (2014).
- 24) K. Cho, H. Kim, M. A. Tanatar, Y. J. Song, Y. S. Kwon, W. A. Coniglio, C. C. Agosta, A. Gurevich, and R. Prozorov, Phys. Rev. B **83**, 060502(R) (2011).
- 25) T. Terashima, K. Kihou, M. Tomita, S. Tsuchiya, N. Kikugawa, S. Ishida, C.-H. Lee, A. Iyo, H. Eisaki, and S. Uji, Phys. Rev. B **87**, 184513 (2013).
- 26) P. Burger, F. Hardy, D. Aoki, A. E. Böhmer, R. Eder, R. Heid, T. Wolf, P. Schweiss, R. Fromknecht, M. J. Jackson, C. Paulsen, and C. Meingast, Phys. Rev. B **88**, 014517 (2013).
- 27) D. A. Zocco, K. Grube, F. Eilers, T. Wolf, and H. v. Löhneysen, Phys. Rev. Lett. **111**, 057007 (2013).
- 28) S. Kittaka, Y. Aoki, N. Kase, T. Sakakibara, T. Saito, H. Fukazawa, Y. Kohori, K. Kihou, C.-H. Lee, A. Iyo, H. Eisaki, K. Deguchi, N. K. Sato, Y. Tsutsumi, and K. Machida, J. Phys. Soc. Jpn. **83**, 013704 (2014).
- 29) M. Kenzelmann, Th. Strässle, C. Niedermayer, M. Sigrist, B. Padmanabhan, M. Zolliker, A. D. Bianchi, R. Movshovich, E. D. Bauer, J. L. Sarrao, and J. D. Thompson, Science **321**, 1652 (2008).
- 30) K. M. Suzuki, Y. Tsutsumi, N. Nakai, M. Ichioka, and K. Machida, J. Phys. Soc. Jpn. **80**, 123706 (2011).
- 31) R. Yoshii, S. Tsuchiya, G. Marmorini, and M. Nitta, Phys. Rev. B **84**, 024503 (2011).
- 32) H. Suhl, B. T. Matthias, and L. R. Walker, Phys. Rev. Lett. **3**, 552 (1959).
- 33) S. Yonezawa, S. Kusaba, Y. Maeno, P. Auban-Senzier, C. Pasquier, K. Bechgaard, and D. Jérôme, Phys. Rev. Lett. **100**, 117002 (2008).
- 34) B. Bergk, A. Demuer, I. Sheikin, Y. Wang, J. Wosnitza, Y. Nakazawa, and R. Lortz, Phys. Rev. B **83**, 064506 (2011).
- 35) M. Takahashi, T. Mizushima, and K. Machida, private communication.
- 36) P. Bak, Rep. Prog. Phys. **45**, 587 (1982).
- 37) M. Chaikin and T. C. Lubensky, *Principles of Condensed Matter Physics* (Cambridge Univ. Press, Cambridge, 1995).
- 38) V. G. Kogan and R. Prozorov, Rep. Prog. Phys. **75**, 114502 (2012).
- 39) R. M. Hornreich, M. Luban, and S. Shtrikman, Phys. Rev. Lett. **35**, 1678 (1975).
- 40) K. Machida and M. Fujita, Phys. Rev. B **30**, 5284 (1984).
- 41) M. Fujita and K. Machida, J. Phys. Soc. Jpn. **53**, 4395 (1984).
- 42) K. Machida, Physica (Amsterdam) **158C**, 192 (1989).
- 43) K. Machida, T. Mizushima, and M. Ichioka, Phys. Rev. Lett. **97**, 120407 (2006).
- 44) T. Mizushima, M. Ichioka, and K. Machida, J. Phys. Soc. Jpn. **76**, 104006 (2007).
- 45) K. Sun and C. J. Bolech, Phys. Rev. A **87**, 053622 (2013).
- 46) K. Sun and C. J. Bolech, Phys. Rev. A **85**, 051607(R) (2012).